Journal of Alloys and Compounds 507 (2010) 429–432

Contents lists available at ScienceDirect

Journal of Alloys and Compounds

journal homepage: www.elsevier.com/locate/jallcom

Synthesis and characterization of KCu_3S_2 microstructures through a composite-hydroxide mediated method

Linyong Huang[a], Jing Liu[a], Zhiyuan Zuo[a], Hong Liu[a,*], Duo Liu[a], Jiyang Wang[a], Robert I. Boughton[b]

[a] State Key Laboratory of Crystal Materials, Shandong University, No. 27 Shandanan Road, Jinan, Jinan 250100, China
[b] Center for Material Science, Bowling Green State University, Bowling Green, OH 43403, USA

ARTICLE INFO

Article history:
Received 21 November 2009
Received in revised form 20 July 2010
Accepted 20 July 2010
Available online 29 July 2010

Keywords:
KCu_3S_2
Synthesis
Micro- and nanostructure
Bandgap

ABSTRACT

KCu_3S_2 microslabs and microbelts have been synthesized using a composite-hydroxide mediated (CHM) approach without the presence of an organic surfactant. X-ray powder diffraction results indicate that the belts possess a monoclinic KCu_3S_2 crystalline structure. Scanning electron microscopy (SEM) and high resolution transmission electron microscopy (HRTEM) were used to obtain detailed characterization of the microstructure and nanostructure of this material. Measurements of the UV–vis absorption spectrum have been performed, and the results reveal that this material is semiconducting with a bandgap of 1.459 eV.

1. Introduction

The ternary K–Cu–S family, including KCu_3S_2 [1], KCu_4S_3 [2], $K_3Cu_8S_6$ [3] and KCu_7S_4 [4] has attracted much research interest over the past 30 years. There is a rich variety of solid state chemistry occurring in these compounds because copper can adopt different coordination numbers [5]. For example, KCu_4S_3 is composed of double layers built up of tetrahedral CuS_4 units that are separated by potassium ions, and KCu_3S_2 is composed of chains with a $[Cu_4S_4]$ column interlinked by two Cu atoms. These chains are also separated by potassium ions. Because the Cu(I) atoms adopt trigonal-planar coordination in the $[Cu_4S_4]$ columns, and the Cu(II) atoms adopt tetrahedral coordination between adjacent $[Cu_4S_4]$ columns, the structure of $K_3Cu_8S_6$ is more like KCu_3S_2. The main difference is that the distance between the $[Cu_4S_4]$ columns is greater because adjacent columns are interlinked by chains consisting of two copper atoms and two sulfur atoms. The KCu_7S_4 structure can be related to that of KCu_3S_2 by interlinking adjacent $Cu_2[Cu_4S_4]$ layers to the columns and then forming a channel structure (see Supplementary information).

Additionally, some of these materials exhibit low temperature phase transitions and resistivity anomalies [4,6–8]. Results of measurements of their electronic properties indicate that mixed-valent KCu_4S_3 and $K_3Cu_8S_6$ are metallic, but that KCu_3S_2 and KCu_7S_4 are semiconductors, for they have no partially filled bands [9,10]. Whangbo and co-workers reported that the resistivity anomalies of $K_3Cu_8S_6$ and KCu_7S_4 at low temperature do not originate from charge density wave instability, but are caused by an order-disorder transition of the Cu^+ ions in the structure [10,11]. Hwu and co-workers proposed a one-dimensional diffusive ordering model that indicates that the phase transition is caused by vacancy ordering involving Cu^+ ion diffusion along the Cu(2)–Cu(2) zigzag chains. They validated this explanation through electron diffraction measurements [12–14]. However, some researchers have noticed that, although the structure of KCu_3S_2 not only possesses the building blocks found in KCu_7S_4, it also possesses the layered structure of $K_3Cu_8S_6$. Ohtani et al. have studied the electrical properties and phase transitions of $TlCu_3S_2$, but not KCu_3S_2 [15]. The properties of KCu_3S_2 have rarely been studied, perhaps because it is difficult to obtain a pure-phase sample of this compound by melting an excess mixture of alkali and sulfur together with copper powder [1]. To the best of our knowledge, up to now there have been no reports of work on the synthesis and characterization of the KCu_3S_2 nanostructure. In this letter, we report on the synthesis and characterization of KCu_3S_2 microstructure and nanostructure through a novel approach. In addition, the optical properties of KCu_3S_2 are investigated.

2. Experimental details

Mass produced KCu_3S_2 with microstructural and nanostructural detail has been obtained by the composite-hydroxide mediated (CHM) approach in the absence of any organic surfactant [16]. A mixture of 0.024 g elemental sulfur and $CuCl_2{\cdot}2H_2O$ at a molar ratio of 3:2 was placed in a Teflon vessel, which also contained 20 g of composited hydroxides (NaOH/KOH = 51.5:48.5). The vessel was then covered by a Teflon cover, and put into a furnace, which was preheated to 230 °C. The hydrox-

* Corresponding author. Tel.: +86 531 88362807; fax: +86 531 88362807.
E-mail address: hongliu@sdu.edu.cn (H. Liu).

0925-8388/$ – see front matter © 2010 Elsevier B.V. All rights reserved.
doi:10.1016/j.jallcom.2010.07.140

ide solution was stirred by shaking the covered vessel to ensure uniformity of the mixed reactants after they were completely molten. After the mixture reacted, the vessel was taken out and cooled to room temperature for 48 h. A one-dimensional KCu_3S_2 belt-like structure was obtained after filtering and washing the product first with deionized water and then with hot water to remove the surface hydroxides. The resulting product was examined by X-ray powder diffraction (XRD) (Bruker D8 Advance with Cu K_α radiation) and field-emission scanning electron microscopy (SEM) (Hitachi S-4800). Detailed microstructural analysis was performed using high resolution transmission electron microscopy (HRTEM) (JEOL JEM-2100) and selected area electron diffraction (SAED). Absorption spectra measurements were performed on a UV–vis near-infrared spectrometer (Hitachi U-3500).

3. Results and discussion

The XRD spectrum of the sample synthesized at 230 °C is shown in Fig. 1. All of the sharp diffraction peaks correspond to monoclinic KCu_3S_2 (the standard JCPDS file No. 34-338 is at the bottom) with lattice parameters of $a = 14.773$ Å, $b = 3.946$ Å and $c = 8.182$ Å. No diffraction peaks from CuS, S or other components were found in the synthesized material. Considering the reagents and products,

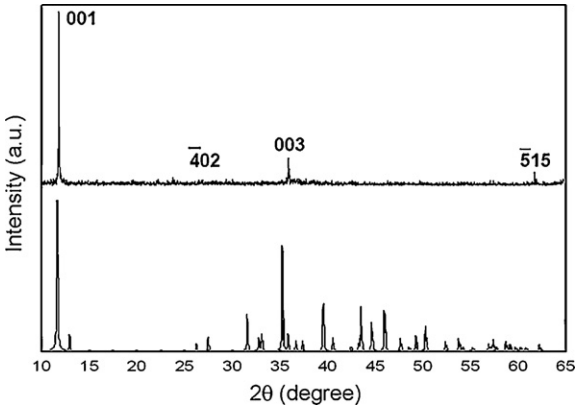

Fig. 1. XRD pattern of the KCu_3S_2 microslabs deposited on Si (0 0 1) substrate.

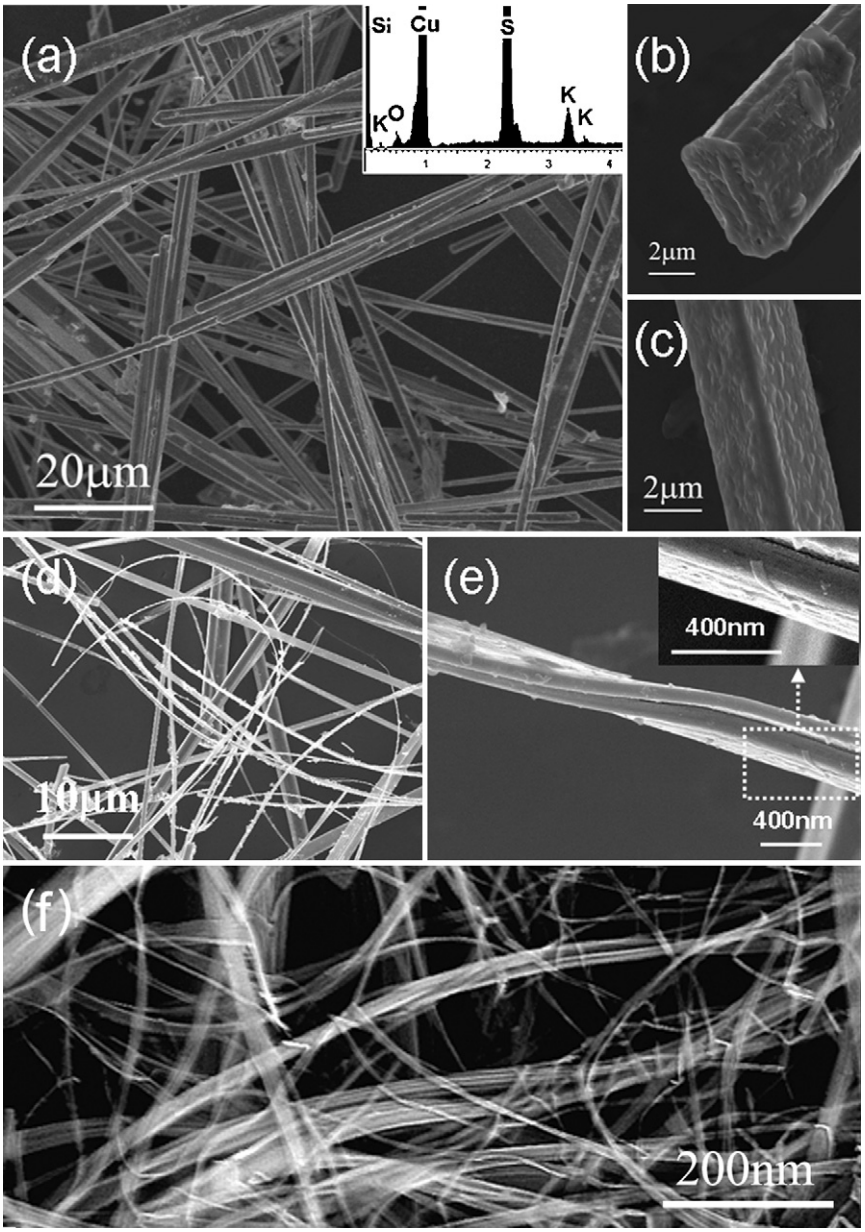

Fig. 2. (a) A low-magnification SEM image of KCu_3S_2 microslabs synthesized at 230 °C, the insert on the upper right is the EDS spectrum of microslabs. (b) The enlarged detail of one end of a KCu_3S_2 microslab. (c) The enlarged detail of the lateral geometry of a KCu_3S_2 microslab. (d) A low-magnification SEM image of some bent KCu_3S_2 microbelts synthesized at 200 °C. (e) The lateral image of a bent belt showing the representative thickness of a single KCu_3S_2 microbelt. (f) Nanobelts obtained by ultrasonic treatment.

we infer that the chemical reaction is:

$$15S + 42KOH + 12CuCl_2 \rightarrow KCu_3S_2 + 24KCl + 7K_2SO_3 + 21H_2O$$

From this reaction, we see that hydroxides not only play a role as solvents for lowering the reaction temperature, but also take part as reactants. In addition, we observe that the (0 0 1) and (0 0 3) peaks of KCu_3S_2 are very strong, a result that reveals that a large number of (0 0 1) crystallographic facets of KCu_3S_2 are exposed in the as-synthesized product.

Fig. 2 shows SEM images of the as-synthesized samples. The product synthesized at 230 °C for 20 h is dominated by slab-like structures with lengths of several-hundred μm up to even longer than 1 mm, widths of several μm and a width-to-thickness ratio of about 2–5 (Fig. 2(a)). The main peak at the starting position and the appearance of the O signal in the EDS pattern (the insert on the upper right of Fig. 2(a)) indicate the presence of a SiO_2 layer on the surface of the Si substrate. The EDS pattern reveals that there are no impurities in these slab-like structures. The slab faces are rectangular (Fig. 2(b)), and the slab edges are curved (Fig. 2(c)), which indicates that they are assembled by combining small building blocks, not single crystals. The width and thickness of the slab-like structures decrease with a decrease in the synthesis temperature. The sample synthesized at 200 °C is composed of belt-like structures. The width of most of the belts is less than 2 μm and the belt thickness ranges from 100 to 200 nm (Fig. 2(d)). From observations on kinked belts (Fig. 2(e)), we note that the belts are comprised of a two-level multilayered structure (insert Fig. 2(e)) that is composed of stacks of a large number of uniform nanobelts of 30-50 nm in thickness and 100–200 nm in width. The thickness of the belt-like structure is the width of the nanobelts. The belt-like structures are easily split into very thin nanobelts under ultrasonic irradiation. Fig. 2(f) shows some nanobelts obtained by ultrasonic treatment for a few minutes. Most microbelts are broken into nanobelts of 30–50 nm in thickness and 100–200 nm in width, dimensions which are consistent with the layer thickness shown in Fig. 2(e). The length of the nanobelt is equivalent to that of the microbelts, indicating that the nanobelts possess high mechanical strength.

TEM and HRTEM images of a KCu_3S_2 nanobelt lying on a TEM grid are shown in Fig. 3. The width of the nanobelt shown in Fig. 3(a) is about 120 nm, which agrees with the SEM observation. Fig. 3b shows an HRTEM image of the nanobelt of Fig. 3(a). The lattice fringe spacing is 3.763 Å, which is about a quarter of the KCu_3S_2 cell parameter (JCPDS No. 34-338). Some vacancies and dislocations are observed in the image. The electron diffraction pattern of the nanobelt (Fig. 3(c)) shows a set of typical KCu_3S_2 (0 1 0) diffraction dots, which reveals that the nanobelt is well crystallized and grows along the (0 1 0) plane. Combining this observation with Fig. 3(a), it is confirmed that the growth direction of the nanobelt is along the [1 0 0] direction, and that it terminates on ±(0 1 0) and ±(0 0 1) crystallographic planes (as illustrated in Fig. 3(d)). Considering the structural properties of KCu_3S_2, the $[Cu_4S_4]$ chains not only form layered units in the (0 0 1) plane, but also form layered units in the (0 1 0) plane (see Supplementary information). However, our results indicate that the strength of the chemical bonds in the (0 1 0) plane is greater than those in the (0 0 1) plane.

Based on the above discussion, a growth mechanism of the microbelts is proposed as follows: crystalline KCu_3S_2 units form layers growing in the (0 1 0) plane along the ±[0 0 1] direction to form nanobelts. Because of the opposite surface charge on opposite sides of the nanobelts, they are easily packed to form micro belts, whose side thickness corresponds to that of the surface plane of the nanobelts [(0 1 0) plane of KCu_3S_2], and whose surface width corresponds to the thickness plane of the nanobelts [(0 0 1) plane of KCu_3S_2]. This is the reason that the (0 0 1) and (0 0 3) peaks are very strong in the XRD pattern of the samples.

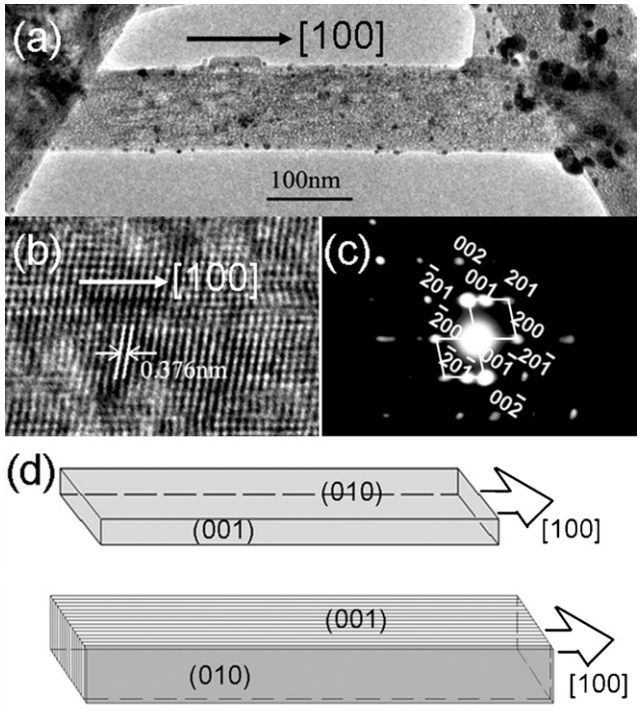

Fig. 3. (a) A low-magnification TEM image of a KCu_3S_2 nanobelt. (b) The selected area HRTEM image of (a). (c) The corresponding electron diffraction pattern of (a). (d) Schematic diagram of the geometrical configuration of a microbelt.

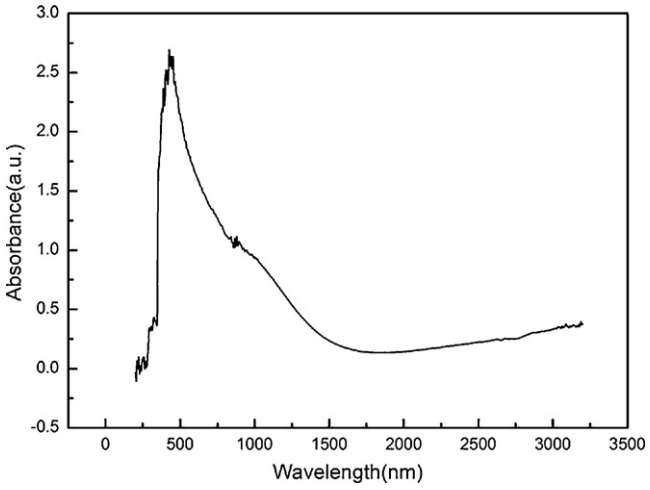

Fig. 4. UV–vis absorption spectrum of KCu_3S_2 at room temperature.

Fig. 4 shows the UV–vis near-infrared absorption spectrum of KCu_3S_2 belts. From this figure, we observe that KCu_3S_2 shows intense absorption at a wavelength of 0.43 μm. The long wave absorption edge of this material is 0.85 μm. Consistent with this absorption edge value, we estimate the bandgap of KCu_3S_2 to be 1.459 eV. The peak appearing at 850 nm is an artifact that was caused by changing the detector.

4. Conclusions

In summary, KCu_3S_2 microbelts and nanobelts were prepared via the composite-hydroxide mediated approach with the absence of any organic surfactants. The microstructure was well characterized by SEM and HRTEM. The HRTEM images reveal that there are numerous defects in the nanobelts. Measurement of the UV–vis

near-infrared absorption spectrum was performed and a bandgap value of about 1.459 eV is calculated from the absorption edge wavelength. This result indicates that the microbelts are semiconductors.

Acknowledgement

This research was supported by NSFC (NSFDYS: 50925205, 50872070, 60974117, IRG, 50721002), and the Program of Introducing Talents of Discipline to Universities in China (111 program).

Appendix A. Supplementary data

Supplementary data associated with this article can be found, in the online version, at doi:10.1016/j.jallcom.2010.07.140.

References

[1] C. Burschka, W. Bronger, Z. Naturforsch. 32B (1977) 11–14.
[2] W. Rudorff, H.G. Schwarz, M.Z. Walter, Anorg. Allg. Chem. 269 (1952) 141–152.
[3] C. Burschka, Z. Naturforsch. 34B (1979) 675–677.
[4] T. Ohtani, J. Ogura, M. Sakai, Y. Sano, Solid State Commun. 78 (1991) 913–917.
[5] H. Boller, J. Alloys Compd. 442 (2007) 3–10.
[6] L.W. ter Haar, F.J. Di Salvo, H.E. Bair, R.M. Fleming, J.V. Waszczak, Phys. Rev. B 35 (1987) 1932–1938.
[7] R.M. Fleming, L.W. ter Haar, F.J. Di Salvo, Phys. Rev. B 35 (1987) 5388–5391.
[8] T. Ohtani, J. Ogura, H. Yoshihara, Y. Yokota, J. Solid State Chem. 115 (1995) 379–389.
[9] D.B. Brown, J.A. Zubieta, P.A. Vella, J.T. Wrobleski, T. Watt, W.E. Hatfield, P. Day, Inorg. Chem. 19 (1980) 1945–1950.
[10] M.-H. Whangbo, E. Canadell, Solid State Commun. 81 (1992) 895–899.
[11] H. Boller, J. Alloys Compd. 480 (2009) 131–133.
[12] K.-S. Lee, D.-K. Seo, M.-H. Whangbo, H. Li, R. Mackay, S.-J. Hwu, J. Solid State Chem. 134 (1997) 5–9.
[13] Y.-K. Kuo, M.J. Skove, D.T. Verebelyi, H. Li, R. Mackay, S. Hwu, M.-H. Whangbo, J.W. Brill, Phys. Rev. B 57 (1998) 3315–3325.
[14] H. Li, R. Mackay, S.-J. Hwu, Y.-K. Kuo, M.J. Skove, Y. Yokota, T. Ohtani, Chem. Mater. 10 (1998) 3172–3183.
[15] T. Ohtani, H. Takeuchi, K. Koh, T. Kaneko, J. Alloys Compd. 317–318 (2001) 201–207.
[16] H. Liu, C.G. Hu, Z.L. Wang, Nano Lett. 6 (2006) 1535–1540.